Exp Fluids (2012) 53:1123–1132
DOI 10.1007/s00348-012-1346-9

RESEARCH ARTICLE

Particle image velocimetry in a foam-like porous structure using refractive index matching: a method to characterize the hydrodynamic performance of porous structures

Denis Butscher · Cédric Hutter · Simon Kuhn · Philipp Rudolf von Rohr

Received: 7 November 2011 / Revised: 27 April 2012 / Accepted: 25 June 2012 / Published online: 18 July 2012
© Springer-Verlag 2012

Abstract We present a method to measure two-dimensional velocity fields inside an artificial foam-like porous structure using particle image velocimetry and a refractive index matching technique to avoid optical distortion. The porous structure is manufactured by stereolithography with the epoxy resin WaterShed® XC 11122 as solid material, and anisole is used as refractive index-matched fluid. It was found that the direction of build-up of the stereolithographic structure plays an important role for the quality of the recorded images. The velocity fields measured in this study and the turbulent statistics derived thereof allow to characterize the hydrodynamic performance of the artificial foam-like structure and clarify the mechanisms of mixing. Results from this study compare well to results from a large eddy simulation reported by Hutter et al. (Chem Eng Sci 66:519–529, 2011b) and hence reinforce these simulations.

List of symbols

A	Cross-sectional area of the empty pipe
D	Empty pipe diameter
n	Number of images
Re	Reynolds number
u, v, w	Components of the instantaneous fluid velocity
u_b	Interstitial bulk velocity
U_b	Bulk velocity
$\dot{V}$	Volumetric flow rate
x, y, z	Cartesian coordinates

D. Butscher · C. Hutter · P. Rudolf von Rohr (✉)
Institute of Process Engineering, ETH Zurich, Sonneggstrasse 3, 8092 Zurich, Switzerland
e-mail: vonrohr@ipe.mavt.ethz.ch

S. Kuhn
Massachusetts Institute of Technology,
77 Massachusetts Avenue, Cambridge, MA 02139, USA

Greek symbols

η	Dynamic viscosity
ρ	Density
Φ	Porosity of the porous structure

Abbreviations

CAD	Computer-aided design
CCD	Charge coupled device
FPIV	Fluorescent particle image velocimetry
LDV	Laser Doppler velocimetry
LES	Large eddy simulation
MRV	Magnetic resonance velocimetry
Nd:YAG	Neodymium:yttrium aluminum garnet ($Y_3Al_5O_{12}$) crystal
PDT	Particle displacement tracking
PIV	Particle image velocimetry
PLIF	Planar laser-induced fluorescence
PMMA	Poly methyl metacrylate
PTV	Particle tracking velocimetry
SL	Stereolithography
SLS	Selective laser sintering

Subscript

b	Bulk quantity
p	Pore quantity

1 Introduction

Motivated by the advantages of continuous manufacturing compared to batch or semi-batch processes widely applied in industry, we developed a new plug flow reactor concept in the millimeter range thereby combining the advantages of the macro- and micro-scale. The reactor is predominately designed for fast and exothermic reactions, and to

provide sufficient mixing, we use highly porous material (metal foams) as static mixers. In a previous study, the mixing efficiency of metal foams with different pore sizes was investigated by combined particle image velocimetry (PIV) and planar laser-induced fluorescence (PLIF) behind the foam (Hutter et al. 2010). It was observed that the turbulence induced by the foam leads to very fast mixing processes at a comparable small pressure drop.

However, the relationship between the geometry of the porous material (e.g. pore size, ligament shape) and the generated turbulence is still not known in detail. Therefore, we designed an artificial foam-like structure with well defined geometry, and we accomplished numerical computations that provide insight into the turbulent transport processes within this porous structure (Hutter et al. 2011b). However, due to the complexity of this problem, these computations need experimental verification. In the present work, we apply a refractive index matching technique to assess the velocity fields by means of PIV within the porous structure in order to address this problem.

2 Literature review

Refractive index matching is a well-established technique to visualize flow fields in packed beds. Northrup et al. (1991) applied fluorescent particle image velocimetry (FPIV) for flow measurements in a packed bed consisting of a poly methyl methacrylate (PMMA) cell with PMMA spheres and a silicon oil mixture as the index-matched fluid. Peurrung et al. (1995) used the same setup to measure velocity fields by means of particle displacement tracking (PDT). In a similar setup, Rashidi et al. (1996) applied PLIF to investigate transport phenomena. A packed bed manufactured from pyrex and the index-matched fluid glycerol was used by Moroni and Cushman (2001) to visualize the flow field by means of particle tracking velocimetry (PTV). Stöhr et al. (2003) used a PMMA box filled with a PMMA or fused silica granulate and an index-matched silicon oil mixture as well as an index-matched zinc chloride solution to visualize the pore-scale flow of two immiscible liquid phases by PLIF. While a packed bed can be simply constructed by filling a tank with granulated material, it is more challenging to manufacture a geometrically defined transparent porous test section for flow investigations. Zerai et al. (2005) built a regular two-dimensional network of flow cells from an acrylic sheet and streamed it with a mixture of sodium iodide solution and glycerin to measure the flow field by PIV. Liu et al. (1990) investigated the flow in the coolant passage of an internal combustion engine cylinder head by streaming a PMMA model with a mixture of hydrocarbon fluids to measure local velocities by means of laser Doppler velocimetry (LDV). In order to manufacture the cylinder head model, they casted PMMA around a fusible core of eutectic alloy that was melted-out after the PMMA cured. Table 1 gives an overview of experimental setups, measurement techniques, and solid/liquid combinations applied in literature to investigate flow phenomena in index-matched complex geometries. A comprehensive overview regarding the arrangement of the experimental setups, selection of solid and liquid materials, and tuning of the properties is given by Budwig (1994). Hassan and Dominguez-Ontiveros (2008) summarized matching refractive index solids and fluids including some of their properties that have been used in index-matched flow studies. A review about refractive index and density matching techniques including a comprehensive list of refractive index-matched fluid recipes is given by Wiederseiner et al. (2011). Up to now, optical flow measurements in complex three-dimensional regular porous structures have not been reported. Furthermore, most of the measurements reported above suffer a low spatial resolution.

Beside optical measurement techniques to visualize flow fields in porous structures, there are also other methods like the magnetic resonance velocimetry (MRV) as reported by Onstad et al. (2011). In their work, they demonstrate the capability of the MRV method to capture temporally averaged three-dimensional flow fields in porous structures with a resolution as high as 0.6 mm. An overview of gamma radiation, X-ray microtomography, and magnetic resonance imaging including advantages, disadvantages,

Table 1 Combinations of solid and liquid material for refractive index-matched flow measurements in porous media

References	Geometry	Technique	Solid material	Liquid
Liu et al. (1990)	Cylinder head model	LDV	PMMA	Hydrocarbon fluids
Northrup et al. (1991)	Packed bed	FPIV	PMMA	Silicon oils
Peurrung et al. (1995)	Packed bed	PDT	PMMA	Silicon oils
Rashidi et al. (1996)	Packed bed	PLIF	PMMA	Silicon oils
Moroni and Cushman (2001)	Packed bed	PTV	Pyrex	Glycerol
Stöhr et al. (2003)	Packed bed	PLIF	PMMA/fused silica	Silicon oils/zinc chloride solution
Zerai et al. (2005)	Flow cell network	PIV	PMMA	Sodium iodide/glycerol/water

and applications is given by Werth et al. (2010). However, all these non-optical methods are not able to record temporally resolved flow fields, and hence, turbulent statistics cannot be accomplished.

3 Experimental setup

In the present study, we demonstrate the capability of the PIV technique in combination with index matching to measure temporally resolved two-dimensional flow fields in a foam-like porous structure with a high spatial resolution. As solid material, we chose the epoxy resin WaterShed® XC 11122 since it can be used for the stereolithographic manufacturing of the complex structure; as refractive index-matched fluid, we used anisole (Sigma–Aldrich).

3.1 Design of artificial foam-like porous structure

The artificial foam-like porous structure investigated in this study resembles the geometry described in Hutter et al. (2011b). For industrial applications, the entire geometry, including the artificial porous structure and the surrounding pipe, can be sintered from a metal alloy in a single piece by the selective laser sintering (SLS) technique, thus generating fixed wall connections that promote the heat transfer from the structure to the pipe (Hutter et al. 2011a). In order to provide optical access, the geometry can also be manufactured from a transparent polymer by stereolitography (SL). With this rapid prototyping technique, a liquid photopolymer is selectively cured by an UV laser, and the desired geometry is formed layer by layer, enabling the manufacturing of almost any geometrically defined shapes and structures. In a previous study (Hutter et al. 2011b), we manufactured this geometry with an inner pipe diameter of 7 mm by SL and analyzed its accuracy using X-ray tomography. Two problems emanating from the SL process become obvious from this scan (Fig. 1): First, the SL technique is not able to generate sharp edges which results in a certain degree of chamfering. As shown in Hutter et al. (2011b), these small changes in the geometry have a strong influence on the flow field and the turbulence induced. Accordingly, the structure design is adjusted by the chamfering of all edges in order to obtain a good agreement between CAD model and the physical SL part. Second, the typical layer thickness of the SL manufacturing process of about 0.1 mm results in a considerable surface roughness that also largely influences the flow dynamics in the structure. As a consequence, the geometry applied in this study was scaled to a pipe inner diameter of 20 mm. Additionally, the internal surfaces were coated with a lacquer to further smoothen the surface and also protect the structure from chemical attack.

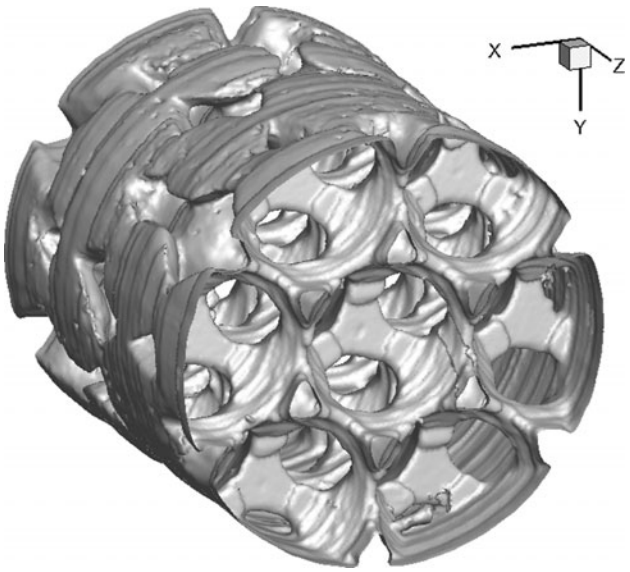

Fig. 1 X-ray scan of the solid wall of an artificial foam-like structure manufactured by stereolithography (SL) with a total diameter of 7 mm

3.2 Test section design and refractive index matching

The geometry of the artificial foam-like structure is the negative pattern of tetrahedral overlapping spheres. The spheres with a diameter of 7.94 mm and a distance of 7.86 mm were subtracted from a cylinder with a diameter of 20 mm to describe a tubular reactor. The unit cell of the foam-like porous structure, as depicted in Fig. 2, consists of 3 layers of cells in axial direction, which represent the periodic unit length of 19.25 mm. All edges are chamfered with a radius of 0.34 mm so that the resulting foam-like structure has a pore size of 2.88 mm and a porosity of $\Phi = 0.78$. The entire geometry consists of 8 unit cells in axial direction.

This structure was integrated in a test section (see Fig. 3) that consists of a pipe with an inner diameter of $D = 20$ mm. The total length of the test section is 354 mm, and the porous structure has an axial extend of 154 mm ($7.7 \cdot D$). To enable optical measurements without distortions by the pipe curvature, the entire test section is manufactured in a rectangular box with plane walls and a quadratic cross-section with an edge length of 30 mm.

The epoxy resin WaterShed® XC 11122 is used as material for the test section; its refractive index is given in Table 2. The advantage of this material is the possibility to use stereolithography for manufacturing. The refractive index matching fluid is anisole, which features the same refractive index as the epoxy resin (see Table 2), and its density and viscosity are almost equal to water.

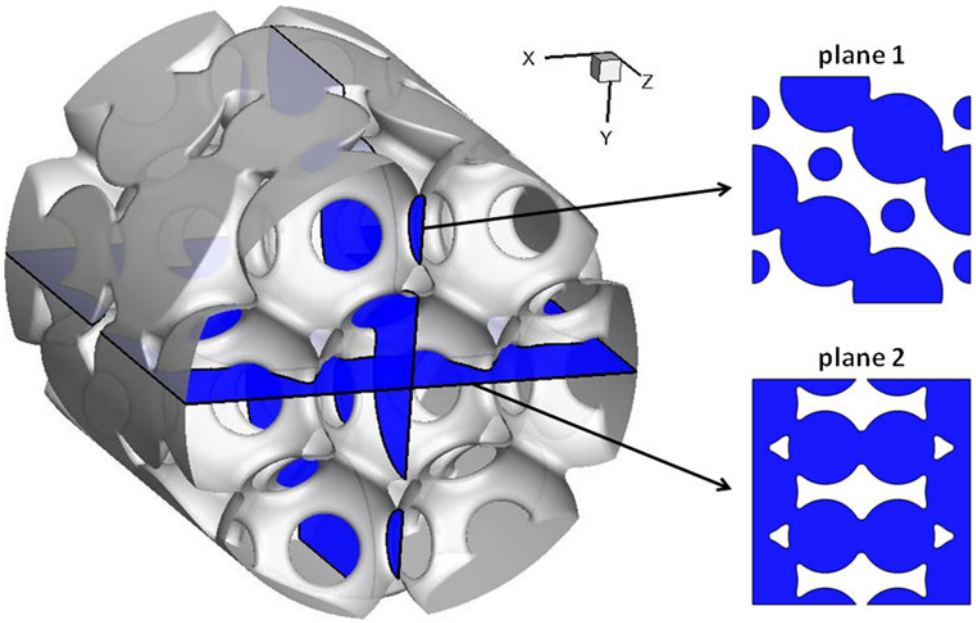

Fig. 2 Representation of the solid walls of the unit cell of the foam-like porous structure with two characteristic planes

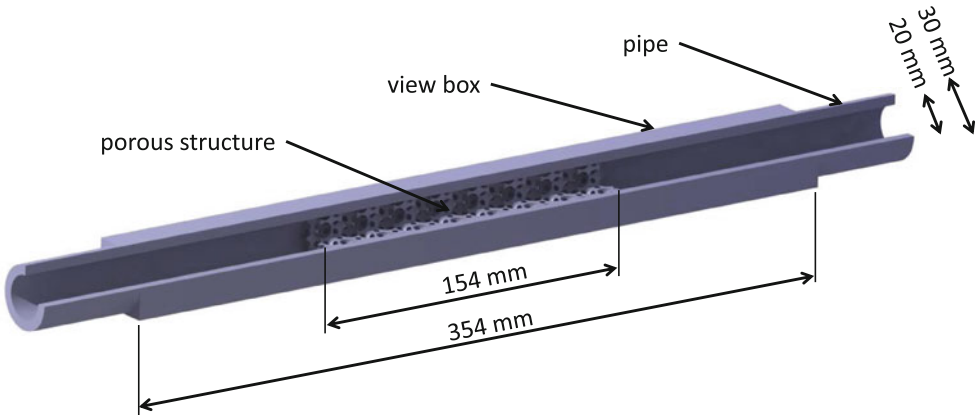

Fig. 3 Test section consisting of the pipe surrounded by a *rectangular view box* and the artificial porous structure inside

Table 2 Properties of WaterShed® XC 11122 and anisole

WaterShed® XC 11122	
Refractive index	1.512–1.515
Anisole[a]	
Density	989 kg/m^3 at 298.15 K
Dynamic viscosity	0.992 mPa s at 298.15 K
Refractive index	1.515

[a] Data taken from Baragi et al. (2005)

A photograph of the test section without and with refractive index matching is depicted in Fig. 4.

The fluid enters the test section, which is mounted vertically, from a straight pipe section with an inner diameter of $D = 20$ mm and a total length of 1,000 mm ($50 \cdot D$) to provide fully developed flow. The entire test facility is a closed loop system consisting of a storage tank,

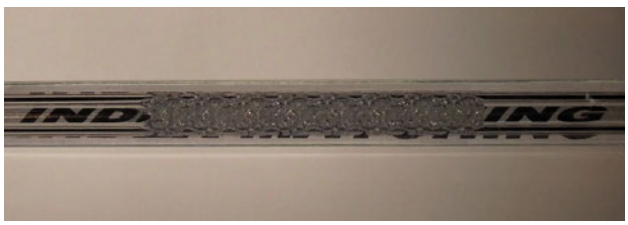

(a) Empty test section

(b) Refractive index matched test section

Fig. 4 Image of the test section without and with refractive index matching

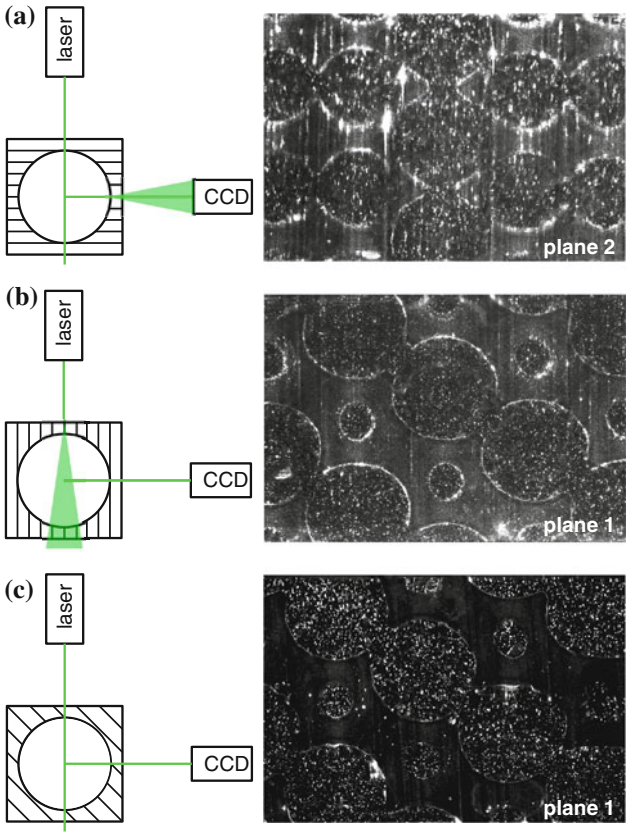

Fig. 5 Influence of the alignment of the laser light sheet and the camera axis to the layers of the structure generated by the stereolithographic fabrication process

a side channel pump, a heat exchanger to remove the heat introduced by the pump, the inlet section where the flow profile can develop, the test section that includes the porous structure, a rotameter to monitor the flow rate, and a thermocouple to record the temperature. The volumetric flow rate is controlled by a frequency converter.

3.3 Light scattering properties of the SL structure

During the manufacturing of the structure, the layer by layer generation of the geometry needs to be taken into account for the optical setup, as it is evident from Fig. 5. A parallel alignment of the camera axis to the layers of the structure (Fig. 5a) yields blurred images. When the layers are parallel to the light sheet and perpendicular to the camera axis, sharp images can be obtained even though the laser sheet suffers from scattering (Fig. 5b). The best results are achieved when the layers of the structure are aligned at an angle of 45° to the camera axis and the light sheet (Fig. 5c). These light scattering properties of the SL structure can be explained by density gradients inside the solid material, resulting from the layer by layer manufacturing process. The energy input of the UV laser used in the curing step is not spatially uniform in depth and thus varies slightly between the individual layers leading to the afore mentioned minor density gradients.

3.4 Image processing and data post-processing

We apply PIV to measure the velocity field in the refractive index-matched porous structure. The laser light source is provided by a flashlamp-pumped dual Nd:YAG-laser (pulse energy 35 mJ), and the light sheet thickness was adjusted to 0.5 mm. The flow is seeded with hollow glass spheres (mean diameter 10 μm, density 1,030 kg/m^3), and the scattered light is recorded with a CCD camera with a pixel resolution of 1,376 × 1,040 pixel^2 equipped with a band-pass filter (532 ± 2 nm) and an objective (focal length 60 mm, relative aperture *f*/8). Due to the large range of velocity magnitudes, special care must be taken when selecting the pulse separation time. The post-processing of the PIV data is comprised of an adaptive cross-correlation algorithm, filtering, and interpolating of the filtered vectors (e.g. Kuhn et al. 2008; Hutter et al. 2010). The area of interest extends over 20 mm × 20 mm, which corresponds to about 1· 10^6 pixel^2 resulting in a spatial resolution of the PIV data of 640 μm given that the interrogation area is 32 × 32 pixel^2 with an overlapping of 50 %.

The uncertainty of the PIV measurements resulting from image acquisition and image processing was estimated to be in the order of 1 % (Hutter et al. 2011b). An additional source of uncertainty emanates from the experimental setup. However, as the image quality is high (see Fig. 5c) and distortion is insignificant, this uncertainty is of minor impact compared to the uncertainty arising from image acquisition and image processing. Finally, we need to take into account the perspective error caused by the out-of-plane particle motion. Based on large eddy simulation (LES) data, we found that this error hardly exceeds 1 % of the bulk velocity for the areas we focus in this work. Especially for regions where the in-plane velocity is pronounced, the perspective error thus is of minor impact.

We consider an ensemble size of 1,000 image pairs at a frame rate of 5 Hz to calculate statistics of the velocity field. To characterize the turbulence induced by the porous structure, we decompose the instantaneous velocity vector $\mathbf{u}$ into a mean velocity $\overline{\mathbf{u}}$ and a fluctuating part $\mathbf{u}'$ (Reynolds 1895)

$$\mathbf{u} = \overline{\mathbf{u}} + \mathbf{u}'. \quad (1)$$

Furthermore, we calculate the root mean square of the velocity fluctuations in each point by averaging over n (n = 1,000) images.

4 Results

Within this study, we performed measurements at a pipe Reynolds number of Re = 2,350 based on the empty tube

diameter and the bulk velocity $U_b = \dot{V}/A$. Therefore, the volumetric flow rate of anisole was adjusted to 2,220 ml/min. The corresponding pore Reynolds number calculated with the pore diameter and the interstitial bulk velocity $u_b = U_b/\Phi$ is $Re_p = 435$. The measurements were performed in two different planes orthogonal to each other (see Fig. 2) in the first three (flow development) and in the seventh (developed flow) periodic unit of the porous structure. In the following, we present the measurement results and compare them to the LES described in Hutter et al. (2011b).

4.1 Velocity fields

The flow enters the test section with a bulk velocity of 0.12 m/s, and the velocity profile at the inlet of the foam structure is fully developed. In Fig. 6, the mean velocity profile measured 20 mm upstream the foam inlet is depicted for the two investigated measurement planes. The profiles are symmetric and in good agreement to each other. They approximately resemble the Hagen–Poiseuille equation describing laminar flow behavior. The flattened profiles in the pipe center indicate that the flow is in the transition regime to turbulent flow, which could be expected given the Reynolds number of $Re = 2{,}350$. Directly in front of the foam, the profile breaks open and recirculation zones are forming at the ligaments where the flow interacts with the solid material. The fluid is accelerating in the pores, and the resulting jets increase the level of turbulent kinetic energy until a developed flow field is observed. This state is already achieved after about 3 periodic lengths. This conclusion was drawn by comparing the flow profiles from plane 2 at the periodic boundary to the first, second, third, and seventh periodic unit as depicted in Fig. 7. Since the inlet profile to the third

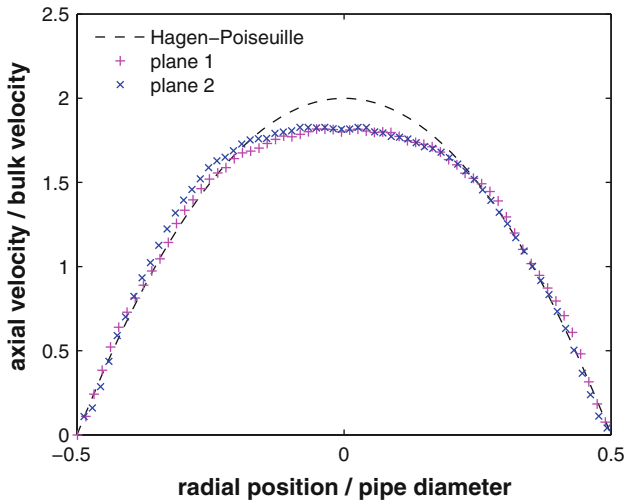

Fig. 6 Velocity profiles upstream the foam inlet at Re = 2,350

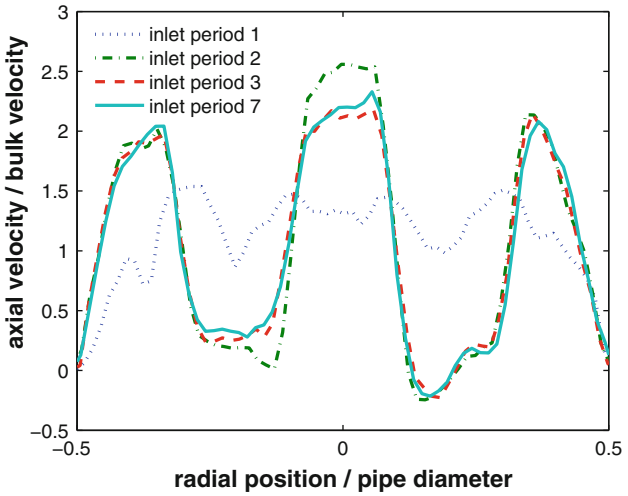

Fig. 7 Temporal mean velocity profiles from plane 2 at the inlet to the first, second third and seventh periodic unit at Re = 2,350

periodic unit is in good agreement to the inlet profile to the seventh periodic unit, the flow can be assumed to be fully developed in this range. To ensure the measurement of a fully developed flow field, the experiments were performed in the 7th period of the test section.

In Fig. 8, a quarter slice of the investigated geometry is demonstrated with the corresponding vector plots of the mean velocity in comparison to the numerical results presented in Hutter et al. (2011b). The experimental data resemble the simulation in many aspects. The separation of the flow at every ligament leading to an enhanced mixing efficiency of the foam element is clearly seen. Also the jets forming through the pores could be detected by PIV. A closer look to a single cell illustrates the reproducibility of the LES results by the PIV measurements. The jet entering the cell through the cut pore is decelerated by recombination processes with the flow through the other pores of the cell. This leads to vortex formation resulting in a complex three-dimensional flow. This flow field could be reproduced with a reasonable agreement to the simulation. Thus, both the vortex on the upper end of the wall, where the fluid leaves the plane of measurement, and the lower end of the cell, where the fluid re-enters the plane, can be seen in the PIV as well as the LES results.

Differences in the flow field are only remarkable near the wall, where the LES has a higher near wall resolution compared to PIV but also relies on wall functions to model this region. Moreover, the PIV data in the outer regions of the measurement domain are affected by the perspective error, which is enhanced in regions where the in-plane velocity component is small compared to the out-of-plane velocity component. Furthermore, we need to mention that the PIV measurements have been performed in an up-scaled geometry compared to the LES grid. Despite

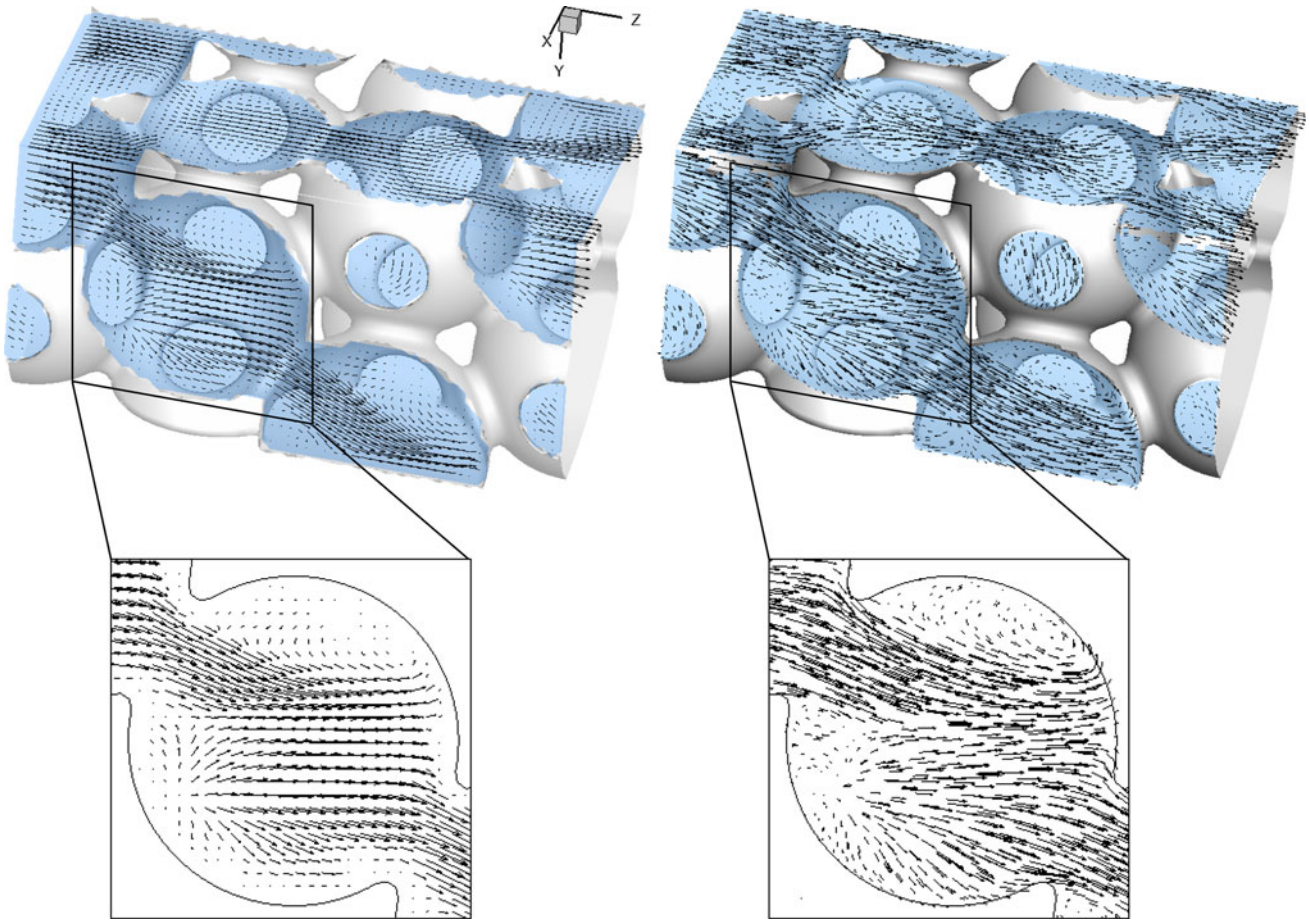

Fig. 8 Velocity vectors (normalized with the bulk velocity and illustrated with same scaling) in both measured planes depicted on a quarter slice of the periodic structure based on PIV data at Re = 2,350 (*left*) and LES data at Re = 2,400 (*right*)

matching the Reynolds number between the experiments and the simulations, there is still a mismatch in the characteristic dimension. Thus, we restrict ourself to a qualitative comparison between PIV and LES, which are observed to be in good agreement.

The contour plots of both planes shown in Fig. 9 compare the numerically estimated mean axial and perpendicular velocity components with the experimental data at similar Reynolds numbers. The velocities are normalized by the bulk velocity in both cases. The perpendicular velocity component is only about 3 times lower than the axial one, and this rather low ratio (compared to classical channel flow) leads to a good convective mass transfer in the geometry as shown in Hutter et al. (2010, 2011c). In the pore ducts, the smallest cross sections of the structure, the highest velocity magnitudes are observed. The zones of increased axial velocity are very distinct and the resulting jets go far into the cells. Downstream the restricting ligaments wakes can be seen. These flow characteristics with alternating velocities were already described in Hutter et al. (2011b). Onstad et al. (2011) were the first to characterize this experimentally in a scaled metal foam replica. In their unstructured material, the flow field is very complex and randomly distributed. Nevertheless, the observed flow phenomena are similar to our investigation.

In addition to the increased contribution of the perpendicular velocity component, the fast development of jets and their dissipation leads to a high level of turbulence. The root mean squares of the axial and perpendicular velocity components estimated from the experimental data and normalized by the bulk velocity are depicted in Fig. 10. One can see from the plots that the magnitude of the RMS values is in the order of the bulk velocity. In the axial RMS values zones of increased fluctuation can be observed arising from the jets entering the cell. This could already be observed in Hutter et al. (2011b). In the perpendicular direction the fluctuation is also very distinct; a homogeneously distributed high level of RMS values can be seen. In comparison to the results of Onstad et al. (2011), we conclude that the radial mixing performance of the designed structure is strongly increased compared to commercial foam due to the higher radial velocity components and the associated higher velocity fluctuations in the stream-wise and its perpendicular directions. This could

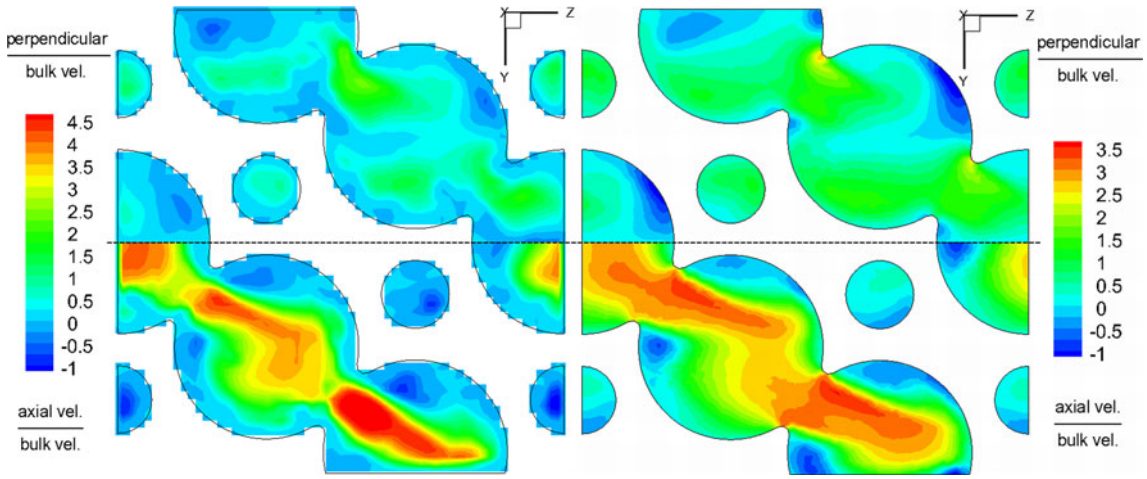

Fig. 9 Axial (*Z* direction) mean velocity field (*bottom*) and perpendicular (*Y* direction) mean velocity field (*top*) from PIV at *Re* = 2,350 (*left*) and LES at *Re* = 2,400 (*right*)

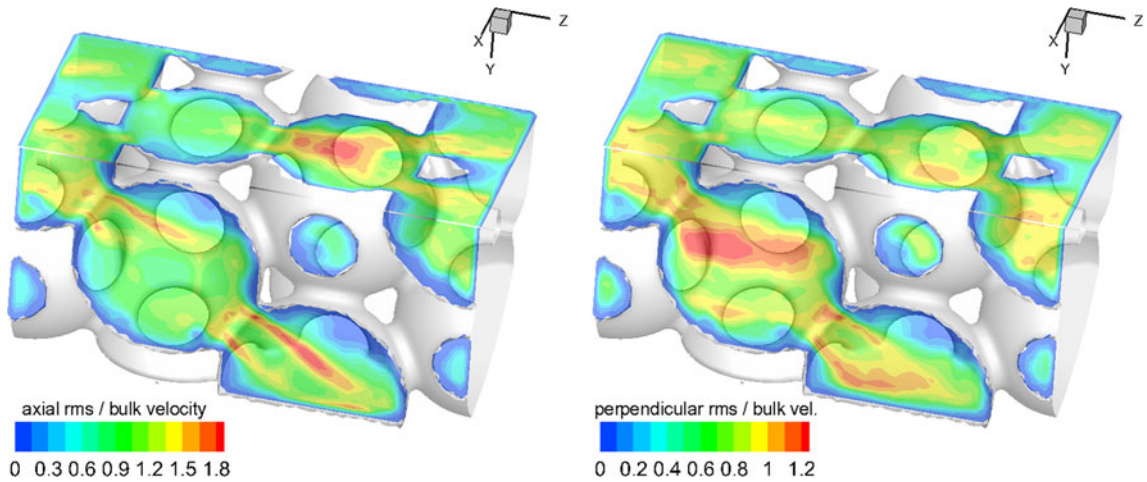

Fig. 10 Axial (*Z* direction) root mean square velocity fields (*left*) and perpendicular (*X*- and *Y*-direction, respectively) root mean square velocity fields (*right*) based on PIV data at *Re* = 2,350

already be shown by the radial mixing experiments presented in Hutter et al. (2011b).

4.2 Coherence length

Onstad et al. (2011) estimated the coherence length of the jets entering a cell from the power spectra of the axial and radial velocity components. These results indicated a coherence length of about 2 times the cell diameter in their unstructured foam. However, in our structured foam, we observe a shorter coherence length, which is quantified by calculating the autocorrelation of the mean streamwise velocity component (Fig. 11). For this procedure, we start at the entrance of a pore and the correlation direction follows the jet development along the centerline of the interconnected pores. It is evident from the figure that after progressing about 80 % of the pore, the initial jet is decayed. This finding is in agreement with the measured and computed mean axial velocity component (see the contour in Fig. 9). Through the interaction of the jet with the jets entering from neighboring cells, it is forced off the centerline, eventually leading to interaction with the pore wall which finally dissipates its energy. This observation is explained by the decreased porosity of our artificial foam geometry and particularly the transverse flow forced by the expert design of the artificial foam-like structure. The reduction of the coherence length of the jets prevents the development of preferential fluid paths. By avoiding such channeling effects, the mass and heat transfer can be increased compared to commercial metal, respectively, ceramic foam. This could be shown by the investigation of Hutter et al. (2010, 2011c).

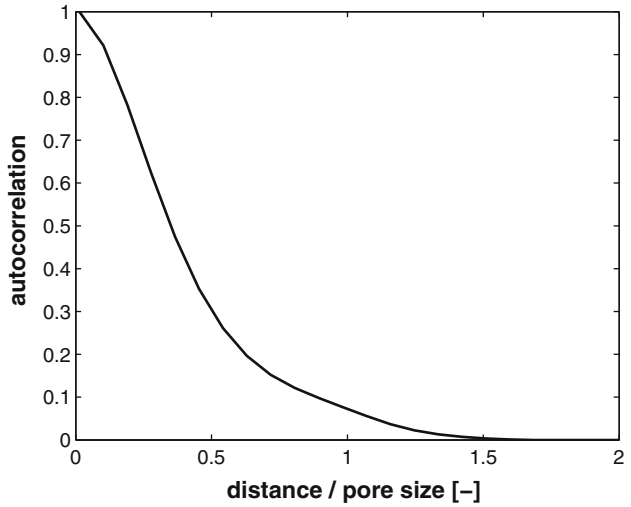

Fig. 11 Autocorrelation of the mean streamwise velocity component of a jet entering the pore along its centerline

5 Conclusions

We presented PIV measurements in a highly complex structure by applying an index matching method. The fluid applied was anisole which is very similar to water in its hydrodynamic properties (density $\rho = 989\,\mathrm{kg/m^3}$, dynamic viscosity $\eta = 0.992$ mPa s). It exhibits the same refractive index (1.515) as the solid material WaterShed® XC 11122 (1.512–1.515), which was used to generate the artificial porous structure by a rapid prototyping method called stereolithography. The designed structure investigated consisted of 8 periodic cells with a mean porosity of $\Phi = 0.78$.

We presented the experimental results of the hydrodynamic characterization at a pore Reynolds number of $Re_p = 435$. The measurements were performed in the 7th periodic unit depicting the fully developed flow field. The experimental data were compared to a LES presented in Hutter et al. (2011b). A good agreement was found between the numerical and experimental results. The mean velocity field could be represented with a high spatial resolution of about 0.64 $\mathrm{mm^2}$. Recombination processes lead to complex flow phenomena in the single cells which increase the level of turbulence in the structure. The large fraction of velocity components perpendicular to the axial direction assists the good convective transport in transverse direction. The fact that the coherence length of the jets forming through the pores is decreased compared to commercial metal, respectively, ceramic foams explains the better performance in heat and mass transfer by avoiding channeling effects. The index matching method gives insight into the temporally and spatially resolved velocity field inside a complex three-dimensional structure. The experimental results allow comparing mean velocity fields and turbulent statistics with numerical simulations that can be applied to optimize the geometry depending on the application.

Acknowledgments We gratefully acknowledge financial support from the Swiss Confederation's innovation promotion agency (CTI) in cooperation with DSM Nutritional Products and Premex Reactor AG.

References

Baragi J, Aralaguppi M, Aminabhavi T, Kariduraganavar M, Kittur A (2005) Density, viscosity, refractive index, and speed of sound for binary mixtures of anisole with 2-chloroethanol, 1,4-dioxane, tetrachloroethylene, tetrachloroethane, dmf, dmso, and diethyl oxalate at (298.15, 303.15, and 308.15) k. J Chem Eng Data 50:910–916

Budwig R (1994) Refractive index matching methods for liquid flow investigations. Exp Fluids 17:350–355

Hassan Y, Dominguez-Ontiveros E (2008) Flow visualization in a pebble bed reactor experiment using PIV and refractive index matching techniques. Nucl Eng Des 238(11):3080–3085

Hutter C, Allemann C, Kuhn S, Rudolf von Rohr P (2010) Scalar transport in a milli-scale metal foam reactor. Chem Eng Sci 65:3169–3178

Hutter C, Büchi D, Zuber V, Rudolf von Rohr P (2011a) Heat transfer in metal foams and designed porous media. Chem Eng Sci 66:3806–3814

Hutter C, Zenklusen A, Kuhn S, Rudolf von Rohr P (2011b) Large eddy simulations of flow through a streamwise-periodic structure. Chem Eng Sci 66:519–529

Hutter C, Zenklusen A, Lang R, Rudolf von Rohr P (2011c) Axial dispersion in metal foams and streamwise-periodic porous media. Chem Eng Sci 66:1132–1141

Kuhn S, Wagner C, Rudolf von Rohr P (2008) The influence of wavy walls on the transport of a passive scalar in turbulent flows. J Turbul 9(10):1–17

Liu C, Vafidis C, Whitelaw J (1990) Flow in the coolant passages of an internal combustion engine cylinder head. Exp Fluids 10:50–54

Moroni M, Cushman JH (2001) Three-dimensional particle tracking velocimetry studies of the transition from pore dispersion to Fickian dispersion for homogeneous porous media. Water Resour Res 37:873–884

Northrup M, Kulp T, Angel S (1991) Fluorescent particle image velocimetry: application to flow measurement in refractive index-matched porous media. Appl Opt 30:3034–3040

Onstad A, Elkins C, Medina F, Wicker R, Eaton J (2011) Full-field measurements of flow through a scaled metal foam replica. Exp Fluids 50:1571–1585

Peurrung LM, Rashidi M, Kulp TJ (1995) Measurement of porous medium velocity fields and their volumetric averaging characteristics using particle tracking velocimetry. Chem Eng Sci 50:2243–2253

Rashidi M, Peurrung L, Tompson AFB, Kulp TJ (1996) Experimental analysis of pore-scale flow and transport in porous media. Adv Water Resour 19:163–180

Reynolds O (1895) On the dynamical theory of incompressible viscous fluids and the determination of the criterion. Philos Trans R Soc Lond Ser A 186:123–164

Stöhr M, Roth K, Jähne B (2003) Measurement of 3D pore-scale flow in index-matched porous media. Exp Fluids 35:159–166

Werth C, Zhang C, Brusseau M, Oostrom M, Baumann T (2010) A review of non-invasive imaging methods and applications in contaminant hydrogeology research. J Contam Hydrol 113:1–24

Wiederseiner S, Andreini N, Epely-Chauvin G, Ancey C (2011) Refractive-index and density matching in concentrated particle suspensions: a review. Exp Fluids 50:1183–1206

Zerai B, Saylor B, Kadambi J, Oliver M, Mazaheri A, Ahmadi G, Bromhal G, Smith D (2005) Flow characterization through a network cell using particle image velocimetry. Transp Porous Media 60:159–181